Environmental Science Nano

ROYAL SOCIETY OF CHEMISTRY

PAPER

View Article Online
View Journal | View Issue



Cite this: *Environ. Sci.: Nano*, 2026, **13**, 2744

# Coppering nanoscale zero-valent iron particles for enhanced decontamination: implications of synthesis conditions on particle architecture and reactivity

Martin Lichovník, *[ab] Miroslav Brumovský, [ac] Jan Filip, [a] Martin Petr [a] and Vojtěch Ettler [b]

Doping of the surface of nanoscale zero-valent iron (nZVI) particles with noble metals enhances their reactivity and efficiency of pollutant removal. In this study, we explored the effects of different synthesis procedures on the performance of Cu-doped nZVI particles in the removal of trichloroethylene (TCE). The abundance, speciation, and distribution of Cu on the Cu–nZVI particle surface were analysed by powder X-ray diffraction (XRD), transmission electron microscopy (TEM) with energy-dispersive X-ray spectroscopy (EDX) mapping, and X-ray photoelectron spectroscopy (XPS). Based on the measurements of oxidation–reduction potential (ORP), pH, and dissolved Cu concentration, a 60 min reaction time was found to be optimal for the Cu–nZVI synthesis. The particles prepared with Cu(II) chloride and sulfate removed 67% more TCE than the non-modified nZVI particles in eight days, degrading it mainly to ethene. In contrast, particles synthesized with Cu(II) nitrate showed no increase the removal efficiency due to (i) higher pH of the dispersions, (ii) more passivated surface, and (iii) the presence of Cu in an amorphous form. Increasing the Cu loading above 1% did not improve the TCE removal rate likely due to the more extensive particle surface passivation. These findings provide insights into optimizing the synthesis and performance of metal-doped (n)ZVI particles for pollutant removal.

Received 23rd July 2025,
Accepted 6th May 2026

DOI: 10.1039/d5en00681c

rsc.li/es-nano



## Environmental significance

Engineered nanomaterials for the removal of (ground)water pollutants show complex relations among their synthesis methods, particle characteristics, and performance. In this study, we demonstrate that the choice of Cu(II) salt used for the surface modification of nanoscale zero-valent iron (nZVI) particles significantly influences their performance in the dechlorination of trichloroethylene (TCE) to the environmentally benign hydrocarbons ethene and ethane. To explain these observations, we conducted a comprehensive material characterisation and evaluated the efficiency and selectivity of the TCE degradation. The key factors controlling the performance were identified as the synthesis pH, surface passivation, and Cu crystallinity. The nZVI particles were synthesized *via* thermal reduction of iron (oxyhydr)oxide precursors—a scalable approach suitable for large-scale production and relevant for field applications.

## 1. Introduction

Nanoscale zero-valent iron (nZVI) particles have been extensively studied over the past 25 years as a promising tool for the removal of a wide range of contaminants from aqueous environments.[1–3] Despite the good reducing and adsorption abilities and the environmental compatibility of nZVI, several challenges continue to impede the widespread adoption of this technology, such as the fast passivation of the nZVI particles in water and their low colloidal stability. Amending the nZVI particles with a small amount of a noble metal, such as palladium, nickel, silver, or copper, has been shown to enhance their reactivity and remediation efficiency.[4] The mechanism of the reactivity enhancement through noble metals in bimetallic nZVI systems is complex and involves the accelerated generation of atomic hydrogen (H*), faster electron transfer through galvanic effects, and improved selectivity due to lower water adsorption affinity at

[a] *Regional Centre of Advanced Technologies and Materials, Czech Advanced Technology and Research Institute (CATRIN), Palacký University Olomouc, Šlechtitelů 27, 779 00 Olomouc, Czech Republic*
[b] *Institute of Geochemistry, Mineralogy and Mineral Resources, Faculty of Science, Charles University, Albertov 6, 128 00 Prague 2, Czech Republic. E-mail: martin.lichovnik@natur.cuni.cz*
[c] *Division of Environmental Geosciences (EDGE), Centre for Microbiology and Environmental Systems Science, University of Vienna, Josef-Holaubek-Platz 2, 1090 Vienna, Austria*

and close to the noble metal atoms.[5–8] Among the noble metals, Pd is often found to be the most effective for improving the (n)ZVI reactivity.[9–11] A more cost-efficient alternative could be the use of Ni.[11–13] Nevertheless, its toxicity presents a limiting factor for its widespread application.[14] The modification of nZVI particles by Cu could, however, provide an effective trade-off between higher efficiency, reasonable cost, and limited toxicity.[9,15–17] Several previous studies showed that amending nZVI with Cu substantially improves the degradation and sequestration of various contaminants, including chlorinated organic pollutants,[11] the antibiotic oxytetracycline,[18] metals and metalloids,[19,20] nitrate,[21,22] and phosphate.[23]

There have been diverse approaches to synthesize the nZVI particles amended with noble metals, resulting in different particle architectures:[24] (i) particles with the noble metal located only within the particle surface (*i.e.*, surface-modified particles) and (ii) particles with the noble metal dispersed in the whole particle volume. Surface-modified particles have been typically prepared by dispersing the previously synthesized nZVI particles in a solution of noble metal salts,[18,21,25] which results in a reductive deposition of noble metals onto the nZVI surface. The particles of the type (ii) can be prepared by coprecipitation from the solutions of Fe(II)/Fe(III) salts in the presence of dissolved noble metals salts by $NaBH_4$.[26,27] The choice of the synthesis method and the type of the particle structure affect the efficiency and mechanism of the pollutant removal.[28,29] The uptake of Cu(II) by nZVI particles is usually fast and efficient, resulting in a facile synthesis of Cu–nZVI particles.[30] In contrast, the uptake of Ni(II) by the nZVI particles is slower and less efficient.[31] A drawback of using metal-doped (n)ZVI particles is the potential oxidation and subsequent release of the second metal to the aqueous phase. Considering Cu-modified (n)ZVI, a significant Cu release has been observed only under acidic conditions.[32,33] However, compared to other metals, the extent of the Cu release from the particles is relatively low.[34]

Trichloroethylene (TCE) is a hazardous anthropogenic pollutant, classified as a human carcinogen (group 1),[35] whose presence in groundwater originates primarily from its industrial use as a degreasing agent and a cleaning solvent. In December 2024, the United States Environmental Protection Agency (US EPA) issued a final rule regulating TCE, which bans its manufacture, processing, and distribution in commerce and introduces stringent worker protection measures for a limited number of TCE uses, which will be phased out over a longer period.[36] Reactive Fe(0)-based materials, such as nZVI, are able to reductively degrade TCE into fully dechlorinated hydrocarbons.[37,38] During the reaction, the nZVI particles are continually transformed into iron (oxyhydr)oxides—natural and non-toxic soil constituents.[39]

Despite extensive research on bimetallic nanoparticles, limited attention has been given to (i) the influence of different salts of the same noble metal on particle synthesis and (ii) the detailed characterization of metal distribution and speciation within such systems. To address these gaps, we synthesized Cu–nZVI particles using three different Cu(II) salts, performed comprehensive material characterization including X-ray diffraction (XRD), elemental mapping *via* transmission electron microscopy (TEM) with energy-dispersive X-ray spectroscopy (EDX), X-ray photoelectron spectroscopy (XPS), and geochemical modelling, and evaluated how these factors affect the TCE dechlorination reactivity. The Cu–nZVI particles were prepared by amending commercially available nZVI with Cu(II) solutions, which represents a simple and scalable approach suitable for field applications.

## 2. Materials and methods

### 2.1 Chemicals

The Cu(II) salts $CuCl_2$ (Sigma-Aldrich, ≥98%), $Cu(NO_3)_2{\cdot}3H_2O$ (Penta, Czech Republic, and Sigma-Aldrich, ≥99%), and $CuSO_4{\cdot}5H_2O$ (Penta, ≥99%) were used for amending the nZVI particles with Cu. The commercially available nZVI powder NANOFER 25P was supplied by NANO IRON (Židlochovice, Czech Republic). The characteristics of the nZVI material and the preparation of the deoxygenated deionized (DO/DI) water are presented in Text S1 in the SI.

### 2.2 Measurement of the oxidation–reduction potential (ORP) and pH during Cu–nZVI synthesis

In a three-neck flask (250 ml), a 20% (w/w) dispersion of nZVI was made using 40 g of nZVI and 80 ml of DO/DI water, followed by 2 min of sonication in an ultrasound bath, and the addition of 80 ml of Cu(II) solution in DO/DI water. The amount of each Cu(II) salt corresponded to a Cu/nZVI mass ratio of 1/100 (*i.e.*, 0.4 g of Cu per 40 g of nZVI). The choice of this Cu/nZVI mass ratio of 1/100 was based on a literature survey (*e.g.*, ref. 16 and 20) and corresponded to a trade-off between the expected effects on the reactivity in comparison to the non-modified nZVI particles and practical applicability. The flask was equipped with a mechanical stirrer (BDC2002 Compact Digital, Caframo, Canada), operating at 300 rpm, pH and ORP probes (details in Text S2), and an injection needle connected to a source of $N_2$ gas. The measurement lasted for 24 h and was carried out in triplicate. The ORP values were recalculated to the standard hydrogen electrode ($E_H$).

### 2.3 Determination of Cu concentration in the aqueous phase during Cu–nZVI synthesis

To study the changes in dissolved Cu concentration during reaction, the Cu–nZVI particles were prepared by mixing 4 g of nZVI powder in 42.2 ml glass vials with 16 ml of a solution of each Cu(II) salt (2500 mg $l^{-1}$ Cu) in DO/DI water. The dispersions were immediately homogenized using a T 18 basic ULTRA-TURRAX dispersion tool (IKA, Germany), operating at 11 000 rpm for 2 min and placed at a vertical rotator (PTR-35, Grant Instruments, UK), operating at 15 rpm. The sample collection and the Cu determination are described in Text S3.

### 2.4 Characterisation of Cu–nZVI particles

The Cu–nZVI particles prepared using three different Cu(II) salts were analysed using a combination of transmission electron microscopy (TEM) with energy-dispersive X-ray spectroscopy (EDX) mapping, powder X-ray diffraction (XRD), and X-ray photoelectron spectroscopy (XPS) to study the nanoparticle composition, morphology, and the distribution and speciation of Cu on the particle surface. The Cu–nZVI dispersions for the particle characterisation were prepared according to the procedure described in section 2.3. After 60 min of reaction, the particles were collected using a permanent magnet and the solution was decanted. The particles were then washed three times with 10 ml of ethanol.

The TEM analysis was performed with a JEM-2100 microscope (JEOL, Japan) coupled with an X-MaxN 80T SDD EDX analyser (Oxford Instruments, United Kingdom) with a drop of the dispersion of the Cu–nZVI particles in ethanol placed on holey carbon-coated gold (Au) grids and evaporated to dryness. Additionally, the distribution of Cu on the surface of nZVI particles, as well as their particle-size and morphology, was investigated by means of transmission electron microscope Titan G2 TEM (FEI, USA), operating at 80 kV and equipped with a BM UltraScan CCD camera (Gatan) and a Super-X EDX system with four silicon drift detectors (Bruker, USA). The EDX elemental maps were collected in a scanning TEM (STEM) mode, with images obtained using the HAADF detector 3000 (Fischione, USA).

The XRD analysis was performed on the particles dried in anoxic conditions using an Empyrean diffractometer (Malvern PANalytical, United Kingdom) equipped with $CoK_\alpha$ radiation source and operating in the Bragg–Brentano geometry with the diffraction patterns acquired in a $2\theta$ range of 5–105° (step size 0.026°, 6 fast scans in 30 min) at ambient conditions. The XRD data were processed using HighScore Plus software (Malvern PANalytical) in conjunction with Crystallography Open Database (COD)[40] and PDF-4+ database.

The XPS analysis was performed using a PHI 5000 VersaProbe II spectrometer (Physical Electronics, USA) with a monochromatic $AlK_\alpha$ radiation source. A small amount of the Cu–nZVI particle dispersion in ethanol was placed on an Al sample holder and immediately inserted into a vacuum chamber of the spectrometer. The measurement was performed at 21 °C and $1.4 \times 10^{-7}$ Pa. The acquisition parameters for the survey spectra were 187.85 eV pass energy and a 1100–0 eV binding energy range with a step of 0.80 eV. For the high-resolution spectra, the pass energy was 23.50 eV, and the spectra were acquired at 0.20 eV steps. Dual beam compensation of the surface charge of the samples was used for each measurement. The evaluation of the acquired spectra was performed with the MultiPak (ULVAC-PHI) software. The values of the binding energies were referenced to the energy of aliphatic carbon (C 1s) at 248.80 eV.

### 2.5 Trichloroethylene degradation experiments

The removal of TCE by Cu–nZVI particles and its degradation products were evaluated in a series of three- and eight-day experiments. The variables tested were the source of Cu (Cu(II) chloride, nitrate, and sulfate), the Cu loading (Cu/nZVI mass ratio of 1/100, 5/100, and 15/100), and the method of mixing Cu(II) solution with nZVI (stirring of the nZVI particles in the Cu(II) solution and continuous addition of the Cu(II) solution during stirring of the nZVI particles in DO/DI water). The concentration of the Cu–nZVI particles was 1 g $l^{-1}$, while the concentration of TCE was 20 mg $l^{-1}$. The detailed experimental protocol is presented in Text S4, together with the description of the subsequent gas chromatography analysis.

To evaluate the selectivity of Cu–nZVI in TCE degradation, we calculated the electron efficiency parameter, $\varepsilon_e$, according to eqn (1),[41] where $p_i$ are the molar quantities of the TCE degradation products multiplied by the respective stoichiometric coefficients, $n_i$, and $p_{H_2}$ is the molar quantity of molecular hydrogen evolved.

$$\varepsilon_e = \frac{\sum n_i p_i}{\sum n_i p_i + 2p_{H_2}} \quad (1)$$

### 2.6 Data treatment and geochemical modelling

The experimental data were plotted using DataGraph 5 software (Visual Data Tools, USA). Where applicable, the measurement uncertainty was expressed as one standard deviation of the analysed replicas. Significant differences among the experimental values were evaluated on the basis of the Tukey–Kramer's honestly significant difference (HSD) test using the One-way ANOVA with *post hoc* Tukey HSD Calculator[42] and, for the data in Table S1 and Cu concentration comparisons in section 3.1, on the basis of the two-sample *t*-test assuming unequal variances using Excel (Microsoft, USA). The PHREEQC-3 geochemical modelling software with the LLNL database[43] was applied on the systems consisting of the solutions of the respective Cu(II) salts (2500 mg $l^{-1}$ Cu) equilibrated with Fe(0). The amounts of Fe(0) used in the calculations were based on the initial nZVI concentration (250 g $l^{-1}$) and the relative abundance of Fe(0) in the (Cu–)nZVI based on the results of the XRD analysis (Fig. 2d).

## 3. Results and discussion

### 3.1 Evolution of $E_H$, pH, and dissolved Cu concentration during the synthesis of Cu–nZVI particles

Fig. 1a shows the evolution of $E_H$ after adding solutions of Cu(II) chloride, nitrate, and sulfate to a freshly prepared nZVI dispersion in DO/DI water. The initial $E_H$ value of the pure DO/DI water was 370 ± 30 mV. An insight into the $E_H$ at the beginning of the reaction is shown in Fig. S1 in the SI. At first, there is a rapid decrease in $E_H$ due to the reactions of nZVI with water, resulting in the formation of molecular hydrogen and hydroxide ions, according to eqn (2).[44]

 

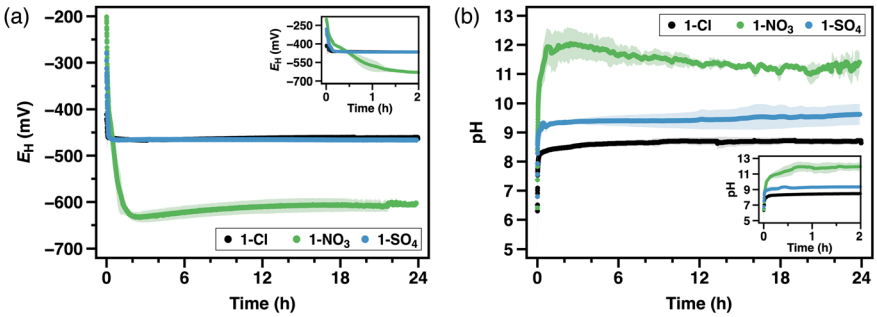


**Fig. 1** Oxidation–reduction potential ($E_H$) (a) and pH (b) in the Cu–nZVI dispersions prepared with different Cu(II) salts. The insets magnify the first 2 h from the beginning of the reaction (*i.e.*, from the addition of the Cu(II) solution to a fresh dispersion of the nZVI particles). The lines of 1-Cl and 1-$SO_4$ in the $E_H$ plot overlap. Lighter colours indicate one standard deviation ($n$ = 3; for 1-$SO_4$, $n$ = 2) calculated for each data point.

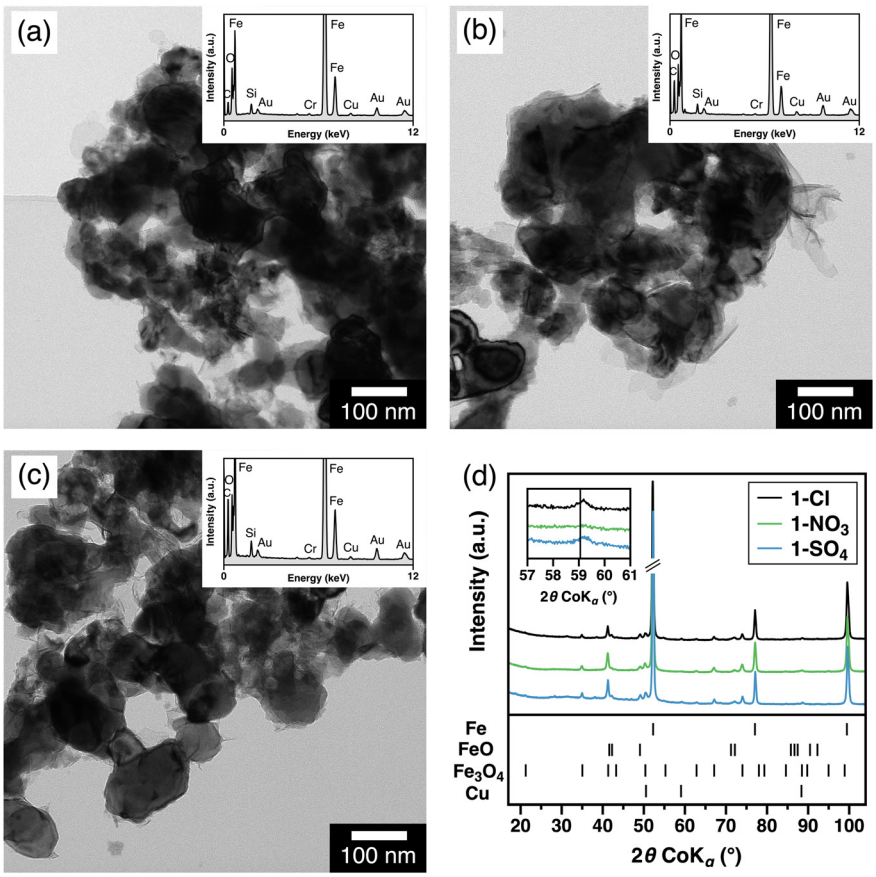


**Fig. 2** Transmission electron micrographs of the Cu–nZVI particles prepared with different Cu(II) salts and a Cu/nZVI mass ratio of 1/100: 1-Cl (a), 1-$NO_3$ (b), and 1-$SO_4$ (c), with the respective energy-dispersive X-ray spectra (insets); and X-ray diffraction patterns of the three samples (d) with an inset magnifying the area of a Cu peak at 59.055° 2$\theta$.

$$Fe + 2H_2O \rightarrow Fe(OH)_2 + H_2 \quad (2)$$

A comparison of the three types of Cu–nZVI reveals considerable similarity for $CuSO_4$ and $CuCl_2$ when used as modifying agents. In both cases, $E_H$ dropped to −465 mV within 15 min after the addition of the Cu(II) solution to the freshly prepared nZVI dispersion. In contrast, the addition of $Cu(NO_3)_2$ to the nZVI dispersion resulted in stronger reducing conditions with slower stabilization of the $E_H$ value. The evolution of $E_H$ in the Cu–nZVI dispersions with nitrate shows three distinct phases: a rapid drop of $E_H$ from the beginning of the reaction to −400 mV within 10 min, followed by a slower decrease to −630 mV within 2 h and a subsequent slight increase up to −610 mV within 24 h. The final $E_H$ value at the end of the initial phase was close to the value of the standard redox potential of the $Fe^{2+}$/Fe couple −447 mV,[45] which is also the case of the Cu–nZVI dispersions with chloride and sulfate. The middle phase was absent in the

case of chloride and sulfate. The stronger reducing conditions in the 1-$NO_3$ dispersion were likely the result of more intense Fe(0) corrosion induced by the presence of easily reducible nitrate ions.[21,22,46,47]

The evolution of the pH during the synthesis of the Cu–nZVI particles, displayed in Fig. 1b and S2, was in agreement with the observed $E_H$. Alkaline conditions emerged from the reaction of the nZVI with water, as mentioned above (eqn (2)). Again, the dispersions with chloride and sulfate showed similar evolution patterns. However, the dispersions with nitrate exhibited a higher pH with a less stable curve. This was likely due to reactions involving the reduction of nitrate ions, which, in contrast to chloride or sulfate ions, can be efficiently reduced by nZVI.[21,22,48] The reduction of nitrate by nZVI is accompanied by an increase in pH, as exemplified in eqn (3).[49]

$$NO_3^- + 3Fe^0 + 3H_2O \rightarrow Fe_3O_4 + NH_4^+ + 2OH^- \quad (3)$$

Although experiments with Fe(0) microparticles have demonstrated only a negligible extent of nitrate removal in unbuffered solutions at an initial pH > 4,[50] the reduction of nitrate by nZVI particles is fast even in unbuffered alkaline solutions.[21] Moreover, the modification of nZVI particles by noble metals may increase the nitrate reduction rate with the effect of the noble metal following the order Cu > Pd > Pt.[21] The typical products of the reduction of nitrate by nZVI particles at low $E_H$ and alkaline pH are mainly ammonium ions ($NH_4^+$) and ammonia ($NH_3$); however, significant amounts of nitrite ($NO_2^-$) have also been observed when Cu–nZVI particles were used.[51]

In addition, the higher pH of the 1-$NO_3$ sample can affect the composition of the outmost iron (oxyhydr)oxide shell due to solubility and low stability of some primary iron-bearing minerals at alkaline pH values, which may promote their dissolution and/or recrystallization into more crystalline secondary minerals.[52] This is likely a contributing factor to the more pronounced formation of magnetite in this sample (see section 3.2).

The Cu concentration in the aqueous phase of the prepared Cu–nZVI dispersions (Table S1 in the SI) decreased from the initial value (nominally 2500 mg $l^{-1}$) in the pure Cu(II) solution to less than 100 μg $l^{-1}$ within the first 5 minutes and remained below 50 μg $l^{-1}$ at the end of the experiment (2 h). A slight increase was observed in the dispersions prepared using Cu(II) chloride and sulfate from 60 to 120 min of the experiment; however, the differences were not statistically significant ($p$ = 0.42 and 0.23, respectively). The uptake of Cu from the solution by the nZVI particles is, therefore, very fast and efficient (>99.99%), being in accordance with previous research.[30,53] The appropriate duration of the modification of the nZVI particles by Cu was estimated from the combination of the above-mentioned experiments. Steady $E_H$ and pH values were established from *ca.* 15 min to 2 h of reaction, depending on the type of the Cu(II) salt used. As a result, a 1-hour reaction time was further used in the synthesis of Cu–nZVI, as within this time, almost all the Cu was removed from the solution.

### 3.2 Characterisation of Cu–nZVI particles by TEM-EDX, XRD, and XPS

Cu–nZVI formed strongly aggregated particles without substantial morphological differences between the particles prepared with different Cu(II) salts (Fig. 2a–c). Using TEM, the Cu on the particle surfaces cannot be distinguished from Fe due to low material contrast. Noble metal doping is not expected to substantially alter the morphology of the nZVI particles at low metal loadings.[29] The reductive deposition mechanism implies that the base metal (Fe) is partly oxidized during the reaction and may subsequently form (oxyhydr) oxides on the particle surface. The morphology of noble metals deposited on the nZVI particle surface has not been widely examined in the literature. Ling and Zhang (2014)[54] reported the formation of discrete Pd clusters on the nZVI particle surface. However, their observations may be affected by the use of ethanol for the preparation of the Pd(II) solution during the synthesis instead of water. The EDX spectra obtained from samples prepared with different Cu(II) salts are shown with the corresponding TEM images in Fig. 2. The copper peaks identified in each spectrum can be ascribed entirely to Cu incorporated in the particles due to the use of Au TEM grids. The presence of Si and Cr in all the samples originates from the impurities of the precursor material used for the nZVI synthesis.

Quantitative phase analysis of the X-ray diffraction patterns based on the Rietveld refinement (Table 1 and Fig. 2d) shows a characteristic composition of the Cu–nZVI samples: a high content of elemental Fe (around 80%), followed by magnetite ($Fe_3O_4$) and wüstite (FeO), its oxidation products (also present in the initial nZVI powder – see section 2.1), and elemental Cu. The amount of Cu in the 1-Cl and 1-$SO_4$ samples corresponded to the theoretical 1/100 Cu/nZVI ratio used to synthesize the particles, while, in the case of the 1-$NO_3$ sample, no Cu was detected. As the experiments involving the measurement of the dissolved Cu concentration during the synthesis indicated almost complete uptake of Cu from the solution by the nZVI particles (see section 3.1 and Table S1), the XRD results suggest that Cu in the Cu–nZVI particles prepared with Cu(II) nitrate is present primarily in an amorphous or nanocrystalline form. The presence of Cu in the 1-$NO_3$ sample was also confirmed by EDX (Fig. 2). The highest amount of magnetite in the 1-$NO_3$ sample correlates with the additional oxidation of Fe(0) by nitrate anions, according to eqn (3).[52]

The XRD analysis of the materials with higher Cu/nZVI mass ratios, *i.e.*, 5/100 and 15/100, also showed the presence of trébeurdenite, a mixed Fe(II)/Fe(III) green rust mineral (Table 1). The presence of trébeurdenite was also observed during the static aging of the nZVI particles in purified water in a previous study.[55] In the 15-Cl sample with the highest Cu/nZVI ratio and the highest chloride concentration in

 

**Table 1** Phase composition (wt%) of Cu–nZVI materials based on the quantitative XRD analysis

| Phase | Formula | 1-Cl | 1-$NO_3$ | 1-$SO_4$ | 5-Cl | 15-Cl | D-5-Cl |
|---|---|---|---|---|---|---|---|
| Iron | Fe | 81.7 | 79.6 | 81.4 | 85.1 | 70.5 | 82.0 |
| Wüstite | FeO | 6.2 | 1.9 | 2.2 | 1.5 | n.d. | 1.3 |
| Magnetite | $Fe_3O_4$ | 11.4 | 18.5 | 15.4 | 9.8 | 11.5 | 9.1 |
| Trébeurdenite | $Fe^{II}_2Fe^{III}_4O_2(OH)_{10}CO_3{\cdot}3H_2O$ | n.d.[a] | n.d. | n.d. | 0.8 | 1.2 | 4.8 |
| Iron(II) hydroxychloride | $Fe^{II}_2(OH)_3Cl$ | n.d. | n.d. | n.d. | n.d. | 5.3 | n.d. |
| Copper | Cu | 0.7 | n.d. | 1.0 | 2.3 | 11.2 | 2.8 |

[a] Not detected.

solution originating from the Cu(II) chloride, Fe(II) hydroxychloride, $Fe_2(OH)_3Cl$, was also detected.

Table 2 presents the composition of the Cu–nZVI particle surface obtained from the XPS analysis. The most abundant elements are O (resulting from the oxidation of the particle surface in the water and sample preparation), Fe, and C (its presence originates partially from ethanol, which was used during sample preparation). The content of Cu is similar for all three Cu–nZVI materials. In the previous analysis by XRD, however, no Cu was detected in the 1-$NO_3$ sample. Considering that Cu in the Cu–nZVI particles is located primarily on their surface and that XRD provides a bulk phase composition, its detection limit is in this case significantly higher than that of XPS in this context. Considering the similar Cu contents across all particle types detected by XPS and the confirmation of Cu incorporation *via* mass balance calculations, these results collectively suggest that Cu in the 1-$NO_3$ sample is present in an amorphous or nanocrystalline form. Small amounts of Si were also detected in the samples, likely due to contamination of the precursor material and/or originating from the glass reaction vessels. High-resolution spectra in the Fe 2p region are displayed in Fig. S3a. The Fe 2p spectra of all three materials contain a component around 706.5 eV, which is indicative of the presence of Fe(0).[56] This component is more pronounced in the 1-Cl and 1-$SO_4$ samples than in the 1-$NO_3$ sample. The surface of the 1-$NO_3$ sample is likely more oxidized due to the reaction with nitrate anions, which is consistent with the results of the XRD analysis (see above). Furthermore, the greater extent of the oxidation of the 1-$NO_3$ surface is supported by the analysis of the O 1s spectra (Fig. S3b). A shoulder at 530 eV, which corresponds to a component of O in the oxides[57] (*i.e.*, mainly Fe oxides/oxyhydroxides in our study), is most pronounced in the 1-$NO_3$ sample.

**Table 2** Surface composition (atomic %) of the non-modified nZVI particles and the Cu–nZVI particles with a 1/100 Cu/nZVI mass ratio prepared using three different Cu(II) salts as determined by X-ray photoelectron spectroscopy (XPS). Small amounts of detected Si were not included in the quantification

| Material | O | Fe | C | Cu | Cl | S |
|---|---|---|---|---|---|---|
| nZVI | 63.6 | 23.7 | 12.7 | n.d.[a] | n.d. | n.d. |
| 1-Cl | 51.5 | 25.0 | 18.0 | 0.7 | 4.7 | n.d. |
| 1-$NO_3$ | 62.6 | 27.6 | 8.8 | 1.0 | n.d. | n.d. |
| 1-$SO_4$ | 59.7 | 26.6 | 10.8 | 1.1 | n.d. | 1.7 |

[a] Not detected.

To examine the spatial distribution of Cu on the surface of Cu–nZVI particles, a Cu–Fe–O EDX elemental mapping was conducted. The resulting images (Fig. 3b and S4) reveal the presence of tiny discrete Cu islands. This structure allows a direct contact of the nZVI core with the surrounding aqueous medium, while the discrete Cu islands can act as catalytic centres.

A comparison of the high-resolution XPS spectra in the Cu 2p region for the three Cu–nZVI samples is displayed in Fig. 3c. As the oxidation state of Cu cannot be identified solely from the positions of the photoelectron lines in the Cu 2p spectra, a complementary analysis of the Cu LMM Auger lines was performed (Fig. 3d). The most prominent line near 568 eV binding energy indicates the presence of Cu primarily as Cu(0) in all the samples.[58] Less intense lines between 569 and 571 eV also suggest the presence of $Cu_2O$.[57] The relative abundance of the Cu species can be determined by the curve-fitting of the Cu LMM spectra.[59] In our study, reliable quantification was, however, not feasible due to the low abundance of Cu and subsequent low signal-to-noise ratio. In previous studies, the chemical form of Cu on the surface of nZVI particles was identified similarly as Cu(0) or $Cu_2O$.[53,60]

Furthermore, the possible reduction of $SO_4^{2-}$ anions on the surface of the Cu–nZVI particles prepared using Cu(II) sulfate was examined. According to the S 2p spectrum of the 1-$SO_4$ sample (Fig. S5), the dominant S species was sulfate; however, reduced S species were also present. The broad line with a maximum at 162.5 eV binding energy was deconvoluted into two components at 162.4 and 163.6 eV ascribed to $2p_{3/2}$ and $2p_{1/2}$ lines of disulfide $(S_2)^{2-}$. The relative abundance of the species was 79% sulfate and 21% disulfide based on the peak area. Although the formation of $Cu_2S$ and CuS is thermodynamically favorable (see below), the high-resolution Cu XPS spectra (Fig. 3c) do not support the presence of these phases. However, similar features have been observed in the analysis of pyrite ($FeS_2$) samples.[61,62] Therefore, the $SO_4^{2-}$ anions appear to have been reduced to form $FeS_2$ or FeS, which is consistent with a recent study that investigated Cu–ZVI materials prepared by ball milling.[63] However, the Fe 2p XPS spectra (Fig. S3a) did not provide sufficient evidence to confirm the presence of the (di-)sulfide phases. In the 1-Cl sample, chlorine was also present, likely

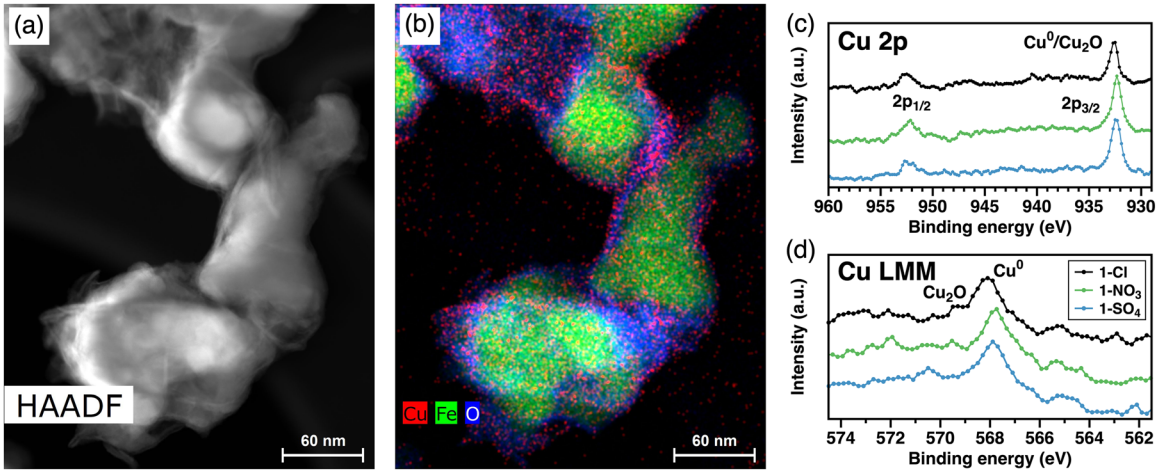


Fig. 3 Transmission electron micrograph of the 1-Cl Cu–nZVI particles (a) with the corresponding energy-dispersive X-ray (EDX) map for Cu, Fe, and O (b); X-ray photoelectron spectroscopy of the three Cu–nZVI materials prepared using different Cu(II) salts (c and d).

as adsorbed $Cl^-$ anions (199.0 eV binding energy of the Cl $2p_{3/2}$ component). No nitrogen was detected in the 1-$NO_3$ sample.

To support the results from the thermodynamic point of view, we calculated the saturation indices of relevant Fe and Cu phases that could be formed during the synthesis of the Cu–nZVI particles. Positive values of the saturation indices displayed in Table S2 indicate the possible reduction of Cu(II) to both Cu(0) and $Cu_2O$ in all the Cu–nZVI dispersions, while the formation of CuO was also possible in the dispersions with Cu(II) nitrate and sulfate. The results also suggest the possibility of the reduction of $SO_4^{2-}$ anions in the dispersion of Fe(0) with Cu(II) sulfate, resulting in the formation of FeS, $FeS_2$, $Cu_2S$, or CuS.

### 3.3 Performance of Cu–nZVI particles in trichloroethylene degradation

**3.3.1 Effects of different Cu(II) salts used for the Cu–nZVI synthesis.** The concentrations of TCE in various Cu–nZVI dispersions measured after three and eight days of reaction are summarized in Fig. 4a and Table S3. After the first three

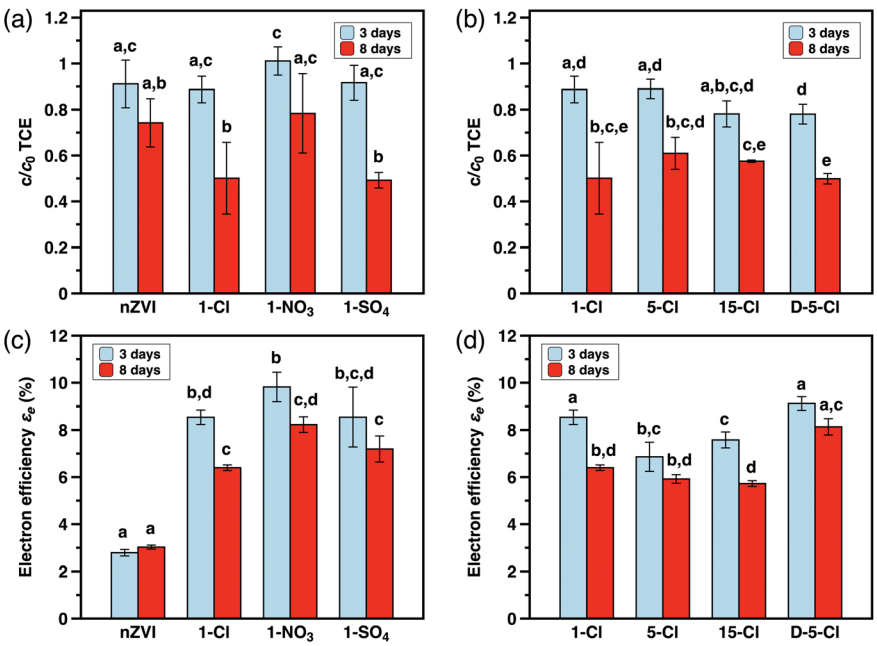


Fig. 4 Relative residual concentration of trichloroethylene (TCE) ($c_0$ = 20 mg $l^{-1}$, corresponding to 152 μmol $l^{-1}$) in the dispersions of nZVI and Cu–nZVI particles prepared with different Cu(II) salts (a) and different Cu loadings (b), after 3 and 8 days of reaction with the corresponding electron efficiencies (c and d). The letters a–e above the columns indicate significant differences ($p < 0.01$ or 0.05) in the mean values within each plot based on the Tukey–Kramer test.

 

days, the amount of TCE in the Cu–nZVI dispersions was not significantly lower than in the dispersion of the non-modified nZVI particles ($p$ = 0.90 for the 1-Cl, $p$ = 0.86 for the 1-$NO_3$, and $p$ = 0.90 for the 1-$SO_4$ sample, respectively). However, larger differences were observed after eight days of reaction: the 1-Cl and 1-$SO_4$ samples removed 50% of the initial TCE amount, while the non-modified nZVI removed only 30%. The 1-$NO_3$ sample showed no improvement in the TCE removal over the non-modified nZVI particles.

Lu *et al.* (2017)[47] suggested that the reason for the lower reactivity of Fe(0) particles toward TCE in the presence of nitrate is the more intense passivation of the iron surface. This correlates with the highest amount of magnetite observed in the 1-$NO_3$ sample by XRD and the lowest amount of Fe(0) in the surface layer as observed by the XPS (see section 3.2, Table 1, and Fig. S3a).

Another factor influencing the removal of TCE by the (Cu–)nZVI particles is the pH. According to the findings of Fan *et al.* (2023),[63] an increase in pH significantly lowers the efficiency of the TCE removal by Cu-modified iron microparticles. In our study, the concentrated dispersions of Cu–nZVI particles prepared with Cu(II) nitrate were highly alkaline (average pH 11.8 after 1 h of reaction, see section 3.1 and Fig. 1b) compared to dispersions with Cu(II) chloride (pH 8.4) and Cu(II) sulfate (pH 9.3). Since the pH was not controlled in our experiments and the particles were used directly from the synthesis mixture without washing, the conditions during the particle synthesis directly impacted the conditions during the experiments. Although the synthesis mixtures were subsequently diluted (from the initial 20 wt.% to 1 g $l^{-1}$ nZVI during the experiments), the higher pH of the 1-$NO_3$ sample may be one of the reasons for its lower reactivity with TCE.

Fan *et al.* (2023)[63] also highlighted the effects of different chemical forms of Cu on the particle surface on the TCE degradation efficiency. They argue that the particles prepared with Cu(II) nitrate are less reactive due to the higher content of $Cu_2O$ on their surface (*i.e.*, high Cu(I)/Cu(0) ratio based on the analysis of the Cu LMM Auger spectra), which, in contrast to Cu(0), does not allow the improvement of particle reactivity *via* galvanic or catalytic effects. Accordingly, the particles prepared with Cu(II) chloride and sulfate exhibited a lower Cu(I)/Cu(0) ratio and, thus, higher reactivity.[63] According to the XPS analysis, all three Cu–nZVI materials contain Cu(0) as the dominant Cu species (Fig. 3c and d). However, the results of the XRD analysis (see section 3.2 and Table 1) revealed the presence of Cu(0) only in the 1-Cl and 1-$SO_4$ samples, indicating that the Cu in the 1-$NO_3$ sample is amorphous/nanocrystalline. Thus, the crystallinity of Cu appears to be an important factor that affects the reactivity of the Cu–nZVI particles toward the TCE. While amorphous metallic phases have shown increased catalytic activity compared to their crystalline counterparts, the lack of order in their structure results in lower electrical conductivity.[64] The less conductive surface of the nZVI particles would, therefore, result in a limited electron transfer from the Fe(0) core. The effect of lowered electrical conductivity, together with a higher pH and a more passivated surface, could explain the lower reactivity of the Cu–nZVI particles prepared using Cu(II) nitrate.

The dominant product of the TCE degradation was ethene for all the Cu–nZVI particle types (Fig. S6), followed by ethane and a minor concentration of 1,1-DCE (*ca.* 1% of the amount of ethene). While similar degradation products were formed, their ratios differed, which can substantially impact the overall degradation efficiency (Fig. S7). The predominance of ethene among the degradation products, together with the absence of acetylene, suggests that Cu doping enhances TCE degradation through both the direct electron transfer and hydrogenolysis *via* adsorbed H* (see Text S5 for a detailed discussion). However, Cu sites are likely not sufficiently active to generate abundant H* for complete hydrogenation, which limits further reduction of ethene to ethane. This is in line with a poor ethene hydrogenation reported for Cu–Fe bimetallic particles[65] and Cu electro-catalysts.[66] In several samples, trace amounts of *cis*- and *trans*-DCE were also detected (data not shown). Neither acetylene nor vinyl chloride (VC) was detected. The absence of the VC intermediate implies its complete conversion into hydrocarbon species. Since only negligible amounts of chlorinated intermediates were detected, it can be concluded that the TCE degradation by Cu–nZVI particles resulted in practically complete dechlorination. Additional discussion and implications regarding the analysis of the TCE degradation products are provided in Text S5 and Fig. S7–S10.

**3.3.2 Effects of higher Cu loadings on the Cu–nZVI reactivity.** Previous studies on granular Fe found a correlation between the increase in bimetallic particle reactivity with pollutants and the noble metal surface coverage.[15,67] These studies found the greatest reactivity enhancement at metal loadings up to the amount necessary for the theoretical formation of one monolayer on the particle surface. In case of the precursor nZVI used in this study, this would correspond to *ca.* 5% Cu loading. However, as the TEM-EDX mapping of Cu–nZVI particles showed that Cu does not form a uniform layer but rather discrete islands (Fig. 3), we decided to also test higher Cu loading of 15%.

The removal of TCE by Cu–nZVI particles with these loadings (*i.e.*, with 5/100 or 15/100 Cu/nZVI mass ratio) is shown in Fig. 4b and Table S3. Interestingly, none of the samples with higher Cu loadings degraded TCE faster than the 1-Cl or 1-$SO_4$ samples with a 1/100 Cu/nZVI mass ratio. The lack of a further increase in removal rate with higher Cu/nZVI ratios may have several explanations: (i) the discrete Cu surface islands may coalesce at higher Cu loadings, blocking access to the reactive Fe(0) surface; (ii) a thicker layer of Fe corrosion products forms on the surface of the nZVI particles as a result of a redox reaction between Fe(0) and Cu(II), which may reduce the rate of electron transfer to the adsorbed pollutant molecules and the generation of H* on the particle surface due to the formation of surface iron (oxyhydr)oxides; (iii) Cu possesses only limited catalytic efficiency for

hydrogen activation compared to Pd or Ni; if sufficient Cu is present to facilitate electron transfer, further increases in Cu likely do not enhance H*-mediated dechlorination; and (iv) higher Cu loadings induced more intense corrosion of the nZVI particles during synthesis, which decreased the nZVI reducing capacity.

Various published studies on the (n)ZVI-based materials modified by Cu have come to different conclusions regarding the effect of Cu loading on their performance in the removal of pollutants (see the extended discussion in Text S6). There is a noticeable difference between granular ZVI and nZVI particles induced by the different amounts of Cu necessary to amend the particle surface with varying specific surface area.

**3.3.3 Electron efficiency ($\varepsilon_e$) and the Cu–nZVI application potential.** In practical applications, the high reactivity of applied nZVI-based treatments toward target pollutants may not be the primary determinant of remedial performance, as nZVI typically reacts readily with water and undergoes rapid corrosion. Electron efficiency, *i.e.*, the percentage of the reducing capacity that can effectively be used for pollutant degradation as opposed to the hydrogen evolution reaction and other side reactions with natural reducible species (see also Text S7), thus represents a crucial performance indicator for nZVI-based materials.[68]

The electron efficiencies of all the Cu–nZVI particles investigated in this study are shown in Fig. 4c and d. The non-modified nZVI particles showed the lowest electron efficiency, reaching 2.9%. The $\varepsilon_e$ values for the Cu–nZVI particles in our study reached >8% in the case of 1-Cl, 1-$NO_3$, 1-$SO_4$, and D-5-Cl after 3 days of reaction. For the 1-$NO_3$ and 1-$SO_4$ samples, the calculation of $\varepsilon_e$ would also need to account for the reduction of nitrate and sulfate ions in the dispersions; these species may be reduced by nZVI and, therefore, should be considered as other side reactions. However, following the results of Schöftner *et al.* (2015),[69] we assumed that the extent of the reduction of sulfate by the nZVI particles was negligible and that the reduction of nitrate occurred mainly during the synthesis of the Cu–nZVI particles, as the process of nitrate reduction is usually fast.[21,22] The values of $\varepsilon_e$ decreased over time, which was likely caused by several factors, including the corrosion of the Fe(0) core of the particles and the spent reduction capacity, and the decrease in the TCE concentration. This observation is essential for the evaluation of the long-term performance of the particles in pollutant degradation. The best stability of $\varepsilon_e$ in time was observed for the D-5-Cl sample (9.1% after 3 days and 8.1% after 8 days of reaction), suggesting a longer reactive lifetime in a practical application. This is likely due to a more uniform distribution of Cu atoms on the particle surface due to the modified synthesis procedure involving the addition of a concentrated Cu(II) solution into a stirred nZVI suspension.

Another important effect that further contributes to the better efficiency of Cu–nZVI particles in the TCE removal compared to the non-modified nZVI particles is the saturation of the product hydrocarbons, expressed as the ethene/ethane ratio (Fig. S7). Although this ratio reached only 2.7 ± 0.4 and 3.0 ± 0.3 for the non-modified nZVI particles after 3 and 8 days of reaction, respectively, for the Cu–nZVI particles, it reached values more than four times larger (*e.g.*, 20.8 ± 0.6 and 13.6 ± 0.8 for the 1-Cl Cu–nZVI particles after 3 and 8 days of reaction, respectively). As the reduction of TCE to ethane requires two electrons more than its reduction to ethene, these results suggest that the Cu–nZVI can degrade an even larger amount of TCE compared to the non-modified nZVI than would be expected solely from the obtained electron efficiency values. Taking into account both electron efficiency and the saturation of product hydrocarbons, the Cu–nZVI particles can degrade up to three times more TCE than the non-modified nZVI (Table S4). Considering the initial concentration of TCE (20 mg $l^{-1}$, *i.e.*, 0.152 mmol $l^{-1}$), the Cu–nZVI particles can degrade up to four times the amount of TCE present in the reaction systems, whereas the non-modified nZVI particles can degrade only around 30% more than the dosed amount of TCE.

Finally, we acknowledge the limitation of using deionized water as a model medium in this study, which does not fully capture the chemical complexity of natural groundwater. Factors such as dissolved minerals, natural organic matter, and variable ionic strength can influence the reactivity, selectivity, and longevity of Cu–nZVI particles. Therefore, long-term batch or column tests with real or simulated groundwater are needed to validate the performance and mechanistic insights observed here under field-relevant conditions.

# 4. Conclusions

Surface modification of the nZVI particles with a small amount of Cu enhances their reactivity and selectivity for TCE degradation. Of the three Cu(II) salts used in our study (chloride, nitrate, and sulfate), Cu(II) chloride and sulfate act similarly in terms of the physicochemical parameters (pH and $E_H$) and material composition (determined primarily by XRD and XPS), resulting in a comparable performance in the TCE degradation. In contrast, the nZVI particles modified by Cu(II) nitrate showed a slower TCE degradation due to the higher pH of the Cu–nZVI dispersions, a more passivated surface, and the presence of Cu in their structure in an amorphous form. Increasing the Cu loading above 1% did not further improve reactivity, likely due to enhanced surface passivation; however, electron efficiency was improved by adding a concentrated Cu(II) solution dropwise to the nZVI dispersion at the Cu/nZVI mass ratio of 5/100 during the stirring rather than mixing directly, suggesting a longer reactive lifetime of the Cu–nZVI particles prepared using this procedure. Overall, our findings show that the choice of the Cu precursor and the synthesis procedure strongly influence the properties of Cu-doped nZVI materials. As similar trends are expected for other noble metals, these insights can be used to improve the reactive lifetime and selectivity of a wide range of noble metal-doped nZVI materials.

 

## Author contributions

ML – data curation, formal analysis, investigation, visualization, writing – original draft. MB – conceptualization, data curation, formal analysis, investigation, methodology, validation, writing – review & editing. JF – conceptualization, funding acquisition, methodology, supervision, writing – review & editing. MP – formal analysis, investigation. VE – funding acquisition, methodology, supervision, writing – review & editing.

## Conflicts of interest

There are no conflicts of interest to declare.

## Data availability

The data for this article have been included as part of the supplementary information (SI) and are also available at Zenodo at https://doi.org/10.5281/zenodo.16368631.

Supplementary information: the SI provides additional details related to the initial nZVI material, the measurement of pH, $E_H$, and Cu concentration, material characterisation techniques, EDX and XPS spectra, TEM images, PHREEQC calculations, and the TCE degradation experiments. See DOI: https://doi.org/10.1039/d5en00681c.

## Acknowledgements

The Palacký University team was supported by the student project IGA_PrF_2019_026 of the Palacký University Olomouc and the Johannes Amos Comenius Programme (P JAC), project No. CZ.02.01.01/00/22_008/0004587, TECHSCALE: Technology beyond nanoscale, under the Ministry of Education, Youth and Sports, Czech Republic (50%; MB, JF, MP). The Charles University team received financial support from the Johannes Amos Comenius Programme, project No. CZ.02.01.01/00/22_008/0004605, Natural and anthropogenic georisks (50%; ML, VE). The authors would like to thank Jana Stráská (TEM), Josef Kašlík (XRD), Ondřej Tomanec (HR-TEM), and Jan Kolařík (laboratory assistance and AAS) at CATRIN. We also thank Vesna Micić Batka and Wolfgang Obermaier at EDGE for assistance in the development of the gas chromatography method and Mr. Alan Harvey Cook for the editing of English in the manuscript. The suggestions of the two anonymous reviewers significantly helped to improve the original manuscript.

## References

1 D. O'Carroll, B. Sleeep, M. Krol, H. Boparai and C. Kocur, Nanoscale zero valent iron and bimetallic particles for contaminated site remediation, *Adv. Water Resour.*, 2013, **51**, 104–122, DOI: 10.1016/j.advwatres.2012.02.005.

2 M. Stefaniuk, P. Oleszczuk and Y. S. Ok, Review on nano zerovalent iron (nZVI): From synthesis to environmental applications, *Chem. Eng. J.*, 2016, **287**, 618–632, DOI: 10.1016/j.cej.2015.11.046.

3 R. Mukherjee, R. Kumar, A. Sinha, Y. Lama and A. K. Saha, A review on synthesis, characterization, and applications of nano zero valent iron (nZVI) for environmental remediation, *Crit. Rev. Environ. Sci. Technol.*, 2016, **46**(5), 443–466, DOI: 10.1080/10643389.2015.1103832.

4 H. J. Lu, J. K. Wang, S. Ferguson, T. Wang, Y. Bao and H. X. Hao, Mechanism, synthesis and modification of nano zerovalent iron in water treatment, *Nanoscale*, 2016, **8**(19), 9962–9975, DOI: 10.1039/c6nr00740f.

5 F. He and D. Zhao, Hydrodechlorination of trichloroethene using stabilized Fe-Pd nanoparticles: Reaction mechanism and effects of stabilizers, catalysts and reaction conditions, *Appl. Catal., B*, 2008, **84**(3–4), 533–540, DOI: 10.1016/j.apcatb.2008.05.008.

6 B. Schrick, J. L. Blough, A. D. Jones and T. E. Mallouk, Hydrodechlorination of Trichloroethylene to Hydrocarbons Using Bimetallic Nickel-Iron Nanoparticles, *Chem. Mater.*, 2002, **14**(12), 5140–5147, DOI: 10.1021/cm020737i.

7 D. M. Cwiertny, S. J. Bransfield and A. L. Roberts, Influence of the Oxidizing Species on the Reactivity of Iron-Based Bimetallic Reductants, *Environ. Sci. Technol.*, 2007, **41**(10), 3734–3740, DOI: 10.1021/es062993s.

8 J. J. White, J. J. Hinsch, W. W. Bennett and Y. Wang, The impact of metal dopants on the properties of nZVI: a theoretical study, *JPhys Mater.*, 2024, **7**, 015013, DOI: 10.1088/2515-7639/ad1c03.

9 Y. H. Kim and E. R. Carraway, Reductive dechlorination of TCE by zero valent bimetals, *Environ. Technol.*, 2003, **24**(1), 69–75, DOI: 10.1080/09593330309385537.

10 T. Zhou, Y. Li and T. T. Lim, Catalytic hydrodechlorination of chlorophenols by Pd/Fe nanoparticles: Comparisons with other bimetallic systems, kinetics and mechanism, *Sep. Purif. Technol.*, 2010, **76**(2), 206–214, DOI: 10.1016/j.seppur.2010.10.010.

11 A. Venkateshaiah, D. Silvestri, S. Wacławek, R. K. Ramakrishnan, K. Krawczyk, P. Saravanan, M. Pawlyta, V. V. T. Padil, M. Černík and D. D. Dionysiou, A comparative study of the degradation efficiency of chlorinated organic compounds by bimetallic zero-valent iron nanoparticles, *Environ. Sci.: Water Res. Technol.*, 2022, **8**(1), 162–172, DOI: 10.1039/D1EW00791B.

12 S. S. Zhang, N. Yang, S. Q. Ni, V. Natarajan, H. A. Ahmad, S. Xu, X. Fang and J. Zhan, One-pot synthesis of highly active Ni/Fe nano-bimetal by simultaneous ball milling and in situ chemical deposition, *RSC Adv.*, 2018, **8**(47), 26469–26475, DOI: 10.1039/c8ra04426k.

13 F. Lin, H. L. Lien, D. T. F. Kuo, K. Wang and Y. Shih, Degradation of pentachlorophenol by CTAB-Modified Ni/Fe Bimetallic Nanoparticles in the Soil Solution, *ACS ES&T Eng.*, 2024, **4**(2), 318–329, DOI: 10.1021/acsestengg.3c00292.

14 E. Denkhaus and K. Salnikow, Nickel essentiality, toxicity, and carcinogenicity, *Crit. Rev. Oncol. Hematol.*, 2002, **42**(1), 35–56, DOI: 10.1016/S1040-8428(01)00214-1.

15 D. M. Cwiertny, S. J. Bransfield, K. J. T. Livi, D. H. Fairbrother and A. L. Roberts, Exploring the Influence of Granular Iron Additives on 1,1,1-Trichloroethane Reduction, *Environ. Sci. Technol.*, 2006, **40**(21), 6837–6843, DOI: 10.1021/es060921v.

16 S. J. Bransfield, D. M. Cwiertny, K. Livi and D. H. Fairbrother, Influence of transition metal additives and temperature on the rate of organohalide reduction by granular iron: Implications for reaction mechanisms, *Appl. Catal., B*, 2007, **76**(3–4), 348–356, DOI: 10.1016/j.apcatb.2007.06.003.

17 R. Wang, T. Tang, G. Lu, Z. Zheng, K. Huang, H. Li, X. Tao, H. Yin, Z. Shi, Z. Lin, F. Wu and Z. Dang, Mechanisms and pathways of debromination of polybrominated diphenyl ethers (PBDEs) in various nano-zerovalent iron-based bimetallic systems, *Sci. Total Environ.*, 2019, **661**, 18–26, DOI: 10.1016/j.scitotenv.2019.01.166.

18 Y. Wu, Q. Yue, Y. Gao, Z. Ren and B. Gao, Performance of bimetallic nanoscale zero-valent iron particles for removal of oxytetracycline, *J. Environ. Sci.*, 2018, **69**, 173–182, DOI: 10.1016/j.jes.2017.10.006.

19 F. Zhu, L. Li, S. Ma and Z. Shang, Effect factors, kinetics and thermodynamics of remediation in the chromium contaminated soils by nanoscale zero valent Fe/Cu bimetallic particles, *Chem. Eng. J.*, 2016, **302**, 663–669, DOI: 10.1016/j.cej.2016.05.072.

20 T. Shubair, O. Eljamal, A. M. E. Khalil, A. Tahara and N. Matsunaga, Novel application of nanoscale zero valent iron and bimetallic nano-Fe/Cu particles for the treatment of cesium contaminated water, *J. Environ. Chem. Eng.*, 2018, **6**(4), 4253–4264, DOI: 10.1016/j.jece.2018.06.015.

21 Y. H. Liou, S. L. Lo, C. J. Lin, W. H. Kuan and S. C. Weng, Chemical reduction of an unbuffered nitrate solution using catalyzed and uncatalyzed nanoscale iron particles, *J. Hazard. Mater.*, 2005, **127**(1–3), 102–110, DOI: 10.1016/j.jhazmat.2005.06.029.

22 J. Guo, P. Guo, M. Yu, Z. Sun, P. Li, T. Yang, J. Liu and L. Zhang, Chemical Reduction of Nitrate Using Nanoscale Bimetallic Iron/Copper Particles, *Pol. J. Environ. Stud.*, 2018, **27**(5), 2023–2028, DOI: 10.15244/pjoes/78439.

23 O. Eljamal, I. P. Thompson, I. Maamoun, T. Shubair, K. Eljamal, K. Lueangwattanapong and Y. Sugihara, Investigating the design parameters for a permeable reactive barrier consisting of nanoscale zero-valent iron and bimetallic iron/copper for phosphate removal, *J. Mol. Liq.*, 2020, **299**, 112144, DOI: 10.1016/j.molliq.2019.112144.

24 K. Mackenzie and A. Georgi, NZVI Synthesis and Characterization, in *Nanoscale Zerovalent Iron Particles for Environmental Restoration: From Fundamental Science to Field Scale Engineering Applications*, ed. T. Phenrat and G. V. Lowry, Springer, Cham, 2019, ch. 2, pp. 45–96, DOI: 10.1007/978-3-319-95340-3_2.

25 W. X. Zhang, C. B. Wang and H. L. Lien, Treatment of chlorinated organic contaminants with nanoscale bimetallic particles, *Catal. Today*, 1998, **40**(4), 387–395, DOI: 10.1016/S0920-5861(98)00067-4.

26 T. W. M. Amen, O. Eljamal, A. M. E. Khalil and N. Matsunaga, Wastewater degradation by iron/copper nanoparticles and the microorganism growth rate, *J. Environ. Sci.*, 2018, **74**, 19–31, DOI: 10.1016/j.jes.2018.01.028.

27 C. Wei, W. Wu, X. Zhao, C. Sun, Z. Shi, J. Yang and M. Wu, Influence of nickel loading on reactivity of Ni/Fe bimetallic nanoparticles toward trichloroethene and carbon tetrachloride, *Environ. Sci.: Nano*, 2025, **2**, 1316, DOI: 10.1039/d4en00426d.

28 Y. Liu, S. A. Majetich, R. D. Tilton, D. S. Sholl and G. V. Lowry, TCE Dechlorination Rates, Pathways, and Efficiency of Nanoscale Iron Particles with Different Properties, *Environ. Sci. Technol.*, 2005, **39**(5), 1338–1345, DOI: 10.1021/es049195r.

29 C. L. Chun, D. R. Baer, D. W. Matson, J. E. Amonette and R. L. Penn, Characterization and Reactivity of Iron Nanoparticles with added Cu, Pd, and Ni, *Environ. Sci. Technol.*, 2010, **44**(13), 5079–5085, DOI: 10.1021/es903278e.

30 A. Liu, J. Fu, J. Liu and W. X. Zhang, Copper Nanostructure Genesis via Galvanic Replacement and Kirkendall Growth from Nanoscale Zero-Valent Iron, *ACS ES&T Eng.*, 2022, **2**(8), 1353–1359, DOI: 10.1021/acsestwater.2c00080.

31 S. Li, W. Wang, F. Liang and W. X. Zhang, Heavy metal removal using nanoscale zero-valent iron (nZVI): Theory and application, *J. Hazard. Mater.*, 2017, **322**, 163–171, DOI: 10.1016/j.jhazmat.2016.01.032.

32 S. Chen, W. Chu, H. Wei, H. Zhao, B. Xu, N. Gao and D. Yin, Reductive dechlorination of haloacetamides in drinking water by Cu/Fe bimetal, *Sep. Purif. Technol.*, 2018, **203**, 226–232, DOI: 10.1016/j.seppur.2018.04.048.

33 L. Fang, C. Xu, W. Zhang and L. Z. Huang, The important role of polyvinylpyrrolidone and Cu on enhancing dechlorination of 2,4-dichlorophenol by Cu/Fe nanoparticles: Performance and mechanism study, *Appl. Surf. Sci.*, 2018, **435**, 55–64, DOI: 10.1016/j.apsusc.2017.11.084.

34 B. Calderon and A. Fullana, Heavy metal release due to aging effect during zero valent iron nanoparticles remediation, *Water Res.*, 2015, **83**, 1–9, DOI: 10.1016/j.watres.2015.06.004.

35 IARC Working Group on the Evaluation of Carcinogenic Risks to Humans, *Trichloroethylene, Tetrachloroethylene, and Some Other Chlorinated Agents*, IARC Monographs on the Evaluation of Carcinogenic Risks to Humans, International Agency for Research on Cancer, Lyon, France, 2014, vol. 106, https://publications.iarc.fr/Book-And-Report-Series/Iarc-Monographs-On-The-Identification-Of-Carcinogenic-Hazards-To-Humans/Trichloroethylene-Tetrachloroethylene-And-Some-Other-Chlorinated-Agents-2014, (accessed March 2024).

36 U.S. Environmental Protection Agency, *Assessing and Managing Chemicals under TSCA. Risk Management for Trichloroethylene (TCE)*, https://www.epa.gov/assessing-and-managing-chemicals-under-tsca/risk-management-trichloroethylene-tce, (accessed October 2025).

37 C. B. Wang and W. X. Zhang, Synthesizing Nanoscale Iron Particles for Rapid and Complete Dechlorination of TCE and PCBs, *Environ. Sci. Technol.*, 1997, **31**(7), 2154–2156, DOI: 10.1021/es970039c.

38 W. A. Arnold and A. L. Roberts, Pathways and Kinetics of Chlorinated Ethylene and Chlorinated Acetylene Reaction with Fe(0) Particles, *Environ. Sci. Technol.*, 2000, **34**(9), 1794–1805, DOI: 10.1021/es990884q.

 

39 C. Coutris, A. Ševců and E. J. Joner, Ekotoxicity of Nanomaterials Used for Remediation, in *Advanced Nano-Bio Technologies for Water and Soil Treatment, Applied Environmental Science and Engineering for a Sustainable Future*, ed. J. Filip, T. Cajthaml, P. Najmanová, M. Černík and R. Zbořil, Springer, Cham, 2020, ch. 28, pp. 573–585, DOI: 10.1007/978-3-030-29840-1_28.

40 S. Gražulis, A. Daškevič, A. Merkys, D. Chateigner, L. Lutterotti, M. Quirós, N. R. Serebryanaya, P. Moeck, R. T. Downs and A. Le Bail, Crystallography Open Database (COD): an open-access collection of crystal structures and platform for world-wide collaboration, *Nucleic Acids Res.*, 2012, **40**(D1), D420–D427, DOI: 10.1093/nar/gkr900.

41 Y. Gu, B. Wang, F. He, M. J. Bradley and P. G. Tratnyek, Mechanochemically Sulfidated Microscale Zero Valent Iron: Pathways, Kinetics, Mechanism, and Efficiency of Trichloroethylene Dechlorination, *Environ. Sci. Technol.*, 2017, **51**(21), 12653–12662, DOI: 10.1021/acs.est.7b03604.

42 N. Vasavada, *One-way ANOVA (ANalysis Of VAriance) with post-hoc Tukey HSD (Honestly Significant Difference) Test Calculator for comparing multiple treatments*, 2016, https://astatsa.com/OneWay_Anova_with_TukeyHSD/.

43 D. L. Parkhurst and C. A. J. Appelo, Description of input and examples for PHREEQC version 3—A computer program for speciation, batch-reaction, one-dimensional transport, and inverse geochemical calculations, *U.S. Geological Survey Techniques and Methods*, 2013, Book 6, ch. A43, p. 497, https://pubs.usgs.gov/tm/06/a43/.

44 J. Filip, F. Karlický, Z. Marušák, P. Lazar, M. Černík, M. Otyepka and R. Zbořil, Anaerobic Reaction of Nanoscale Zerovalent Iron with Water: Mechanism and Kinetics, *J. Phys. Chem. C*, 2014, **118**(25), 13817–13825, DOI: 10.1021/jp501846f.

45 P. Vanýsek, Electrochemical series, in *CRC Handbook of Chemistry and Physics*, ed. W. M. Haynes, CRC Press, Boca Raton, FL, 97th edn, 2016, ch. 5, pp. 78–84.

46 O. Schlicker, M. Ebert, M. Fruth, M. Weidner, W. Wüst and A. Dahmke, Degradation of TCE with Iron: The Role of Competing Chromate and Nitrate Reduction, *Groundwater*, 2000, **38**(3), 403–409, DOI: 10.1111/j.1745-6584.2000.tb00226.x.

47 Q. Lu, S. W. Jeen, L. Gui and R. W. Gillham, Nitrate reduction and its effects on trichloroethylene degradation by granular iron, *Water Res.*, 2017, **112**, 48–57, DOI: 10.1016/j.watres.2017.01.031.

48 Y. Feng, X. Huang, Z. Y. Wu, H. Wang, K. Zuo and Q. Li, Polarity Modulation Enhances Electrocatalytic Reduction of Nitrate by Iron Nanocatalysts, *ACS ES&T Eng.*, 2024, **4**(4), 928–937, DOI: 10.1021/acsestengg.3c00507.

49 A. M. E. Khalil, O. Eljamal, S. Jribi and N. Matsunaga, Promoting nitrate reduction kinetics by nanoscale zero valent iron in water via copper salt addition, *Chem. Eng. J.*, 2016, **287**, 367–380, DOI: 10.1016/j.cej.2015.11.038.

50 C. P. Huang, H. W. Wang and P. C. Chiu, Nitrate reduction by metallic iron, *Water Res.*, 1998, **32**(8), 2257–2264, DOI: 10.1016/S0043-1354(97)00464-8.

51 Y. H. Hwang, D. G. Kim and H. S. Shin, Mechanism study of nitrate reduction by nano zero valent iron, *J. Hazard. Mater.*, 2011, **185**(2–3), 1513–1521, DOI: 10.1016/j.jhazmat.2010.10.078.

52 K. Sohn, S. W. Kang, S. Ahn, M. Woo and S. K. Yang, Fe(0) Nanoparticles for Nitrate Reduction: Stability, Reactivity, and Transformation, *Environ. Sci. Technol.*, 2006, **40**(17), 5514–5519, DOI: 10.1021/es0525758.

53 D. Karabelli, Ü. Çağri, T. Shahwan, A. E. Eroğlu, T. B. Scott, K. R. Hallam and I. Lieberwirth, Batch Removal of Aqueous Cu2+ Ions Using Nanoparticles of Zero-Valent Iron: A Study of the Capacity and Mechanism of Uptake, *Ind. Eng. Chem. Res.*, 2008, **47**(14), 4758–4764, DOI: 10.1021/ie800081s.

54 L. Ling and W. X. Zhang, Structures of Pd–Fe(0) bimetallic nanoparticles near 0.1 nm resolution, *RSC Adv.*, 2014, **4**(64), 33861, DOI: 10.1039/c4ra04311a.

55 J. Semerád, J. Filip, A. Ševců, M. Brumovský, N. H. A. Nguyen, J. Mikšíček, T. Lederer, A. Filipová, J. Boháčková and T. Cajthaml, Environmental fate of sulfidated nZVI particles: the interplay of nanoparticle corrosion and toxicity during aging, *Environ. Sci.: Nano*, 2020, **7**, 1794–1806, DOI: 10.1039/D0EN00075B.

56 M. C. Biesinger, B. P. Payne, A. P. Grosvenor, L. W. M. Lau, A. R. Gerson and R. S. C. Smart, Resolving surface chemical states in XPS analysis of first row transition metals, oxides and hydroxides: Cr, Mn, Fe, Co and Ni, *Appl. Surf. Sci.*, 2011, **257**(7), 2717–2730, DOI: 10.1016/j.apsusc.2010.10.051.

57 N. S. McIntyre and D. G. Zetaruk, X-ray photoelectron spectroscopic studies of iron oxides, *Anal. Chem.*, 1977, **49**(11), 1521–1529, DOI: 10.1021/ac50019a016.

58 I. Platzman, R. Brener, H. Haick and R. Tannenbaum, Oxidation of Polycrystalline Copper Thin Films at Ambient Conditions, *J. Phys. Chem. C*, 2008, **112**(4), 1101–1108, DOI: 10.1021/jp076981k.

59 M. C. Biesinger, Advanced analysis of copper X-ray photoelectron spectra, *Surf. Interface Anal.*, 2017, **49**(13), 1325–1334, DOI: 10.1002/sia.6239.

60 X. Li and W. X. Zhang, Sequestration of Metal Cations with Zerovalent Iron Nanoparticles – A Study with High Resolution X-ray Photoelectron Spectroscopy (HR-XPS), *J. Phys. Chem. C*, 2007, **111**(19), 6939–6946, DOI: 10.1021/jp0702189.

61 M. Descostes, F. Mercier, N. Thromat, C. Beaucaire and M. Gautier-Soyer, Use of XPS in the determination of chemical environment and oxidation state of iron and sulfur samples: constitution of a data basis in binding energies for Fe and S reference compounds and applications to the evidence of surface species of an oxidized pyrite in a carbonate medium, *Appl. Surf. Sci.*, 2000, **165**(4), 288–302, DOI: 10.1016/S0169-4332(00)00443-8.

62 Y. Mikhlin, A. Romanchenko and Y. Tomashevich, Surface and interface analysis of iron sulfides in aqueous media using X-ray photoelectron spectroscopy of fast-frozen dispersions, *Appl. Surf. Sci.*, 2021, **549**, 149261, DOI: 10.1016/j.apsusc.2021.149261.

63 B. Fan, B. Zhou, S. Chen, F. Zhu, B. Chen, Z. Gong, X. Wang, C. Zhu, D. Zhou, F. He and S. Gao, Preparation of Fe/Cu bimetals by ball milling iron powder and copper sulfate for trichloroethylene degradation: Combined effect of FeSx and Fe/Cu alloy, *J. Hazard. Mater.*, 2023, **460**, 132402, DOI: 10.1016/j.jhazmat.2023.132402.

64 Y. Zhou and H. J. Fan, Progress and Challenge of Amorphous Catalysts for Electrochemical Water Splitting, *ACS Mater. Lett.*, 2021, **3**(1), 136–147, DOI: 10.1021/acsmaterialslett.0c00502.

65 F. He, Z. Li, W. Xu, H. Sheng, Y. Gu, Y. Jiang and B. Xi, Dechlorination of Excess Trichloroethene by Bimetallic and Sulfidated Nanoscale Zero-Valent Iron, *Environ. Sci. Technol.*, 2018, **52**(15), 8627–8637, DOI: 10.1021/acs.est.8b01735.

66 B. Schmid, C. Reller, S. S. Neubauer, M. Fleischer, R. Dorta and G. Schmid, Reactivity of Copper Electrodes towards Functional Groups and Small Molecules in the Context of $CO_2$ Electro-Reductions, *Catalysts*, 2017, **7**(5), 161, DOI: 10.3390/catal7050161.

67 S. J. Bransfield, D. M. Cwiertny, A. L. Roberts and D. H. Fairbrother, Influence of Copper Loading and Surface Coverage on the Reactivity of Granular Iron toward 1,1,1-Trichloroethane, *Environ. Sci. Technol.*, 2006, **40**(5), 1485–1490, DOI: 10.1021/es051300p.

68 D. Fan, D. M. O'Carroll, D. W. Elliott, Z. Xiong, P. G. Tratnyek, R. L. Johnson and A. Nunez Garcia, Selectivity of Nano Zerovalent Iron in In Situ Chemical Reduction: Challenges and Improvements, *Rem. J.*, 2016, **26**(4), 27–40, DOI: 10.1002/rem.21481.

69 P. Schöftner, G. Waldner, W. Lottermoser, M. Stöger-Pollach, P. Freitag and T. G. Reichenauer, Electron Efficiency of NZVI Does Not Change with Variation of Environmental Parameters, *Sci. Total Environ.*, 2015, **535**, 69–78, DOI: 10.1016/j.scitotenv.2015.05.033.

 